Influence of misfit and interfacial binding energy on the shape of the oxide precipitates in metals; Interfaces between Mn3O4 precipitates and Pd studied with HRTEM

Kooi, Bart; De Hosson, J.T.M.

Publication date:
2000

[Link to publication in University of Groningen/UMCG research database](#)

INFLUENCE OF MISFIT AND INTERFACIAL BINDING ENERGY ON THE SHAPE OF THE OXIDE PRECIPITATES IN METALS; INTERFACES BETWEEN Mn_3O_4 PRECIPITATES AND Pd STUDIED WITH HRTEM

B. J. KOOI and J. Th. M DE HOSSON*

Department of Applied Physics, Materials Science Centre and Netherlands Institute for Metals Research, University of Groningen, Nijenborgh 4, 9747 AG Groningen, The Netherlands

Abstract—Transmission electron microcopy (TEM) revealed Mn_3O_4 precipitates with two types of dominant shape in Pd–3at.% Mn that was internally oxidized in air at 1000°C. One type is octahedrally shaped and bounded by {111} planes of the Mn_3O_4. These observations were compared with earlier observations in the Ag/Mn_3O_4 system and the octahedrons show a relatively larger truncation by (002) in Pd than in Ag. Further, the second type of precipitate shape, comprising about 1/3 of all of the precipitates in Pd, was not observed in Ag. It corresponds to a plate-like structure, showing an orientation relationship where the tetragonal axes of Mn_3O_4 are parallel to the cube axes of Pd, with the c-axis of Mn_3O_4 as habit plane normal. High-resolution TEM observations revealed the presence of a square misfit dislocation network with line direction $\langle 110 \rangle$ and Burgers vector $1/2\langle 110 \rangle$ at these interfaces with $(002)Mn_3O_4 \| \{200\}Pd$. The general conclusions of the present analysis are: (1) the anisotropy in interface energy for oxide precipitates in a metal matrix is substantial due to the ionic nature of the oxide, giving well-defined shapes associated with the Wulff construction; (2) the influence of misfit energy on the precipitate shape as bounded by semi-coherent interfaces is important only if sufficient anisotropy in mismatch is present and if the matrix is sufficiently stiff; and (3) the stronger coupling strength due to electronic binding effects across the interface in Pd compared with Ag is responsible for formation of the dislocation network structures at larger misfit. © 2000 Acta Metallurgica Inc. Published by Elsevier Science Ltd. All rights reserved.

Keywords: Transmission electron microscopy (TEM); Composites; Metals; Oxides; Dislocations; Interface

1. INTRODUCTION

The mechanical properties of metal-matrix composite materials at the macroscopic scale are, to a large extent, controlled by the microstructure of the metal/ceramic interfaces. Detailed knowledge of the microstructure and chemistry of these interfaces at an atomic level is helpful for tailoring the properties of composite materials for advanced applications. High-resolution transmission electron microscopy (HRTEM) is particularly suited to obtain information about the atomic structure of interfaces. Interfaces between ceramic precipitates that are in an equilibrium state in a metal matrix reflect the balance between interfacial energy and strain energy [1]. As a result, the study of these interfaces may provide insight into the factors responsible for the stability of interfaces.

The equilibrium shape of small inclusions [speci-fied by the orientation relationship (OR) together with interface orientations (IOs)] is determined by both interfacial energy and strain energy. In the absence of strain, a construction analogous to Wulff's [2], based on a polar plot of interface energy as a function of interface normal, provides uniquely the equilibrium shape of the precipitate [3]. Depending on the magnitude of the stress/strain, the elastic energy can become appreciable and result in deviations of the equilibrium shape associated with the Wulff construction. In some systems strain can be the dominant factor controlling the shape. Such systems can be found in the class of coherent metallic inclusions in a metal matrix in the presence of anisotropic strains. Then, the equilibrium shape can be predicted by approaches based on minimization of elastic strain energy [4–9]. Closely related approaches, although based on geometrical arguments, involve the search for invariant planes [10, 21] or invariant lines [12–16]. In the determination of the OR together with the habit plane between precipitate and matrix, in general the precipitate and matrix are related by a Bain–strain lattice

---

* To whom all correspondence should be addressed. E-mail: hossonj@phys.rug.nl.

correspondence [10, 11]. One (real-space) direction with small or zero mismatch where the other two orthogonal directions have large mismatch favours needle precipitates [5, 15] and for reverse mismatch favours plate precipitates [4, 13]. Systems with tetragonal strains may thus serve to verify the relative importance of the influence of mismatch on precipitate shape.

For face-centred cubic (fcc)/body-centred cubic (bcc) and hexagonal close-packed (hcp)/bcc systems where the two types of crystal structure can be related by a Bain–strain lattice correspondence, it is shown that the invariant-line criterion can explain observed ORs and habit planes [12–16]. These systems comprise metal, metal nitride and metal carbide inclusions in metal matrices. Apparently, minimizing misfit (at least along one direction) is important and even dominant with respect to the factors causing anisotropy in the interfacial binding energy. In contrast to the above systems, not much is known about the relative importance of misfit on the shape of *oxide* precipitates in metal matrices. Compared with the metal and the largely covalent nitride and carbide inclusions mentioned above, oxides may behave totally differently because they generally have a predominantly ionic character. The ionicity leads to the occurrence of polar and non-polar interfaces where screening of the metal and image charges in the metal play an important role [17, 18]. Therefore, anisotropy in interfacial binding energy is expected to be much more pronounced for ionic than for the other types of precipitate.

Most of the work on oxide precipitates in a metal matrix was conducted on NaCl-type oxides (e.g. MgO, MnO, NiO, CdO) in an fcc metal matrix [19–27]. These systems are not interesting for studying the relative importance of misfit on the shape of oxide precipitates, since an isotropic mismatch between precipitate and matrix is present. In this respect Mn_3O_4 becomes interesting, because it is related to the NaCl-type oxides in the sense that the fcc O sublattice is tetragonally distorted with a c/a ratio of 1.157. So, apart from the expected strong anisotropy in interfacial binding energy, also a strong anisotropy in misfit is added for the system of Mn_3O_4 precipitates in an fcc metal matrix and hence the competition between these two factors can be studied. In our previous work the influence of tetragonality on the precipitate shape and interface structure, i.e. particularly the misfit dislocation structure at the interfaces, of Mn_3O_4 precipitates in an Ag or Cu matrix was addressed [28–31]. For the investigations presented in this paper, the Ag (or Cu) matrix was replaced by a Pd matrix. It will be shown that a comparison of these different systems gives important clues about the balance between the interfacial binding energy and the misfit energy in determining the stability of (semi-coherent) metal/oxide interfaces.

2. EXPERIMENTAL

An alloy of Pd containing 3 at.% Mn starting from the pure constituents (99.99% by weight) was prepared in an arc furnace. The button was homogenized for 5 days at a temperature of 850°C in an evacuated quartz tube. Subsequently it was cold rolled from 5 mm down to 0.3 mm. Manganese oxide precipitates within Pd were obtained by oxidizing the alloy in air at 1000°C for times ranging between 2 and 10 days. The alloy oxidized for 2 days was also annealed for 1 week in an evacuated quartz tube at 1000°C to allow equilibration to occur.

Samples for (HR)TEM investigations were obtained by cutting 3 mm discs from the 0.3 mm foil with an NdYag laser, followed by grinding, dimpling (Gatan model 656) and ion milling (Gatan PIPS model 691). For (HR)TEM, a JEOL 4000 EX/II instrument operating at 400 kV was used (spherical aberration coefficient, 0.97±0.02 mm; defocus spread, 7.8±1.4 nm; beam semi-convergence angle, 0.8 mrad).

3. RESULTS

According to selected-area electron diffraction (SAED) patterns and HRTEM images, internal oxidation of Pd–3 at.% Mn in air at 1000°C results in Mn_3O_4 precipitates. Other phases of manganese oxide were not observed. Mn_3O_4 possesses a tetragonally distorted spinel crystal structure with a-axes of 0.814 nm and c-axis of 0.942 nm [32]. In fact, the crystal structure is I4/amd with the a-axes $1/2\sqrt{2}$ times 0.814 nm and the c-axis 0.942 nm, where the a-axes of tetragonal spinel and I4/amd are related by a rotation of 45° around the c-axis. However, to allow for a logical and close comparison between the face-centred tetragonal (fct) O sublattice of Mn_3O_4 and the fcc lattice of Pd, here the larger tetragonally distorted spinel unit cell will be used as the crystallographic basis for Mn_3O_4.

Fig. 1 shows a bright-field TEM image of an Mn_3O_4 precipitate in Pd as viewed along their common ⟨110⟩ direction, together with the corresponding SAED pattern. The Mn_3O_4 precipitate is bounded by two pairs of edge-on observed {111} and one pair of edge-on observed (002). Hence, the Mn_3O_4 has its long c-axis in the plane of projection. The SAED pattern shows that the {111} of Mn_3O_4 are aligned parallel to the {111} of Pd for only one pair of facets. For the other pair of {111} facets, a tilt of 7.6° around the ⟨110⟩ viewing direction is present between the {111} planes of Pd and Mn_3O_4. Between the (002) of Mn_3O_4 and Pd a tilt of 3.8° occurs. Fig. 2(a) and (b) shows HRTEM images of parts of the 7.6°-tilted and parallel {111} Mn_3O_4/Pd interfaces, respectively. At the tilted interface [Fig. 2(a)] ledges in the Pd with direction ⟨110⟩ (viewing direction) and height 1/4⟨112⟩ (perpendicular to the interface plane and the viewing direction) can be observed with a mutual distance of
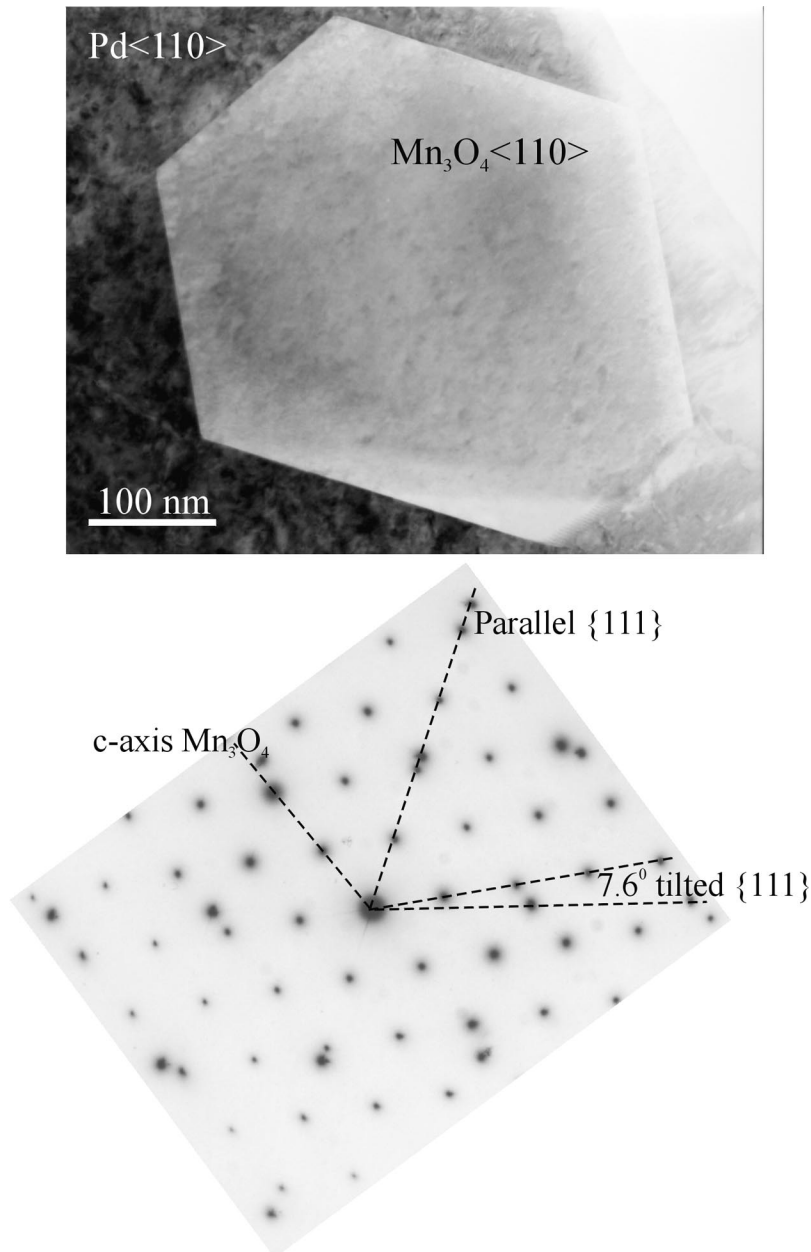
Fig. 1. Bright-field TEM image (top) and corresponding SAED pattern (bottom) of an (002)-truncated, octa-hedrally shaped Mn_3O_4 precipitate in Pd as viewed along their common $\langle 110 \rangle$ axis (note that this is the only common direction for Mn_3O_4 and Pd). For one pair of facets {111} planes of Mn_3O_4 and Pd are aligned parallel and then for the other pair of facets their {111} planes show a mutual tilt of 7.6° (where the tilt axis is parallel to the $\langle 110 \rangle$ viewing direction).

seven to eight Pd {111} planes, making a large angle with the interface.

Due to the tetragonality of Mn_3O_4, only one or two directions and planes can be simultaneously parallel to the ones in Pd. Parallelism of the principal axes of Mn_3O_4 and the cube axes of Pd implies that a tilt of 3.8° is present between all four pairs of {111} of Mn_3O_4 and Pd. This orientation is observed for Mn_3O_4 in Pd, but much less frequently than the orientation shown above where the Mn_3O_4 is rotated

around a $\langle 110 \rangle$ (perpendicular to the c-axis) to bring {111} of Mn_3O_4 and Pd parallel for one pair of facets. The reason why the orientation with one pair of parallel and one pair of 7.6°-tilted facets is energetically more favourable than two pairs of 3.8°-tilted facets is obviously related to the concave-shaped cusp in energy for deviations from the parallel alignment (see Fig. 3). Note that, for the orientation with four pairs of 3.8°-tilted interfaces, only 1/3 of the $\langle 110 \rangle$ directions of Pd and Mn_3O_4 are parallel (i.e. the two of
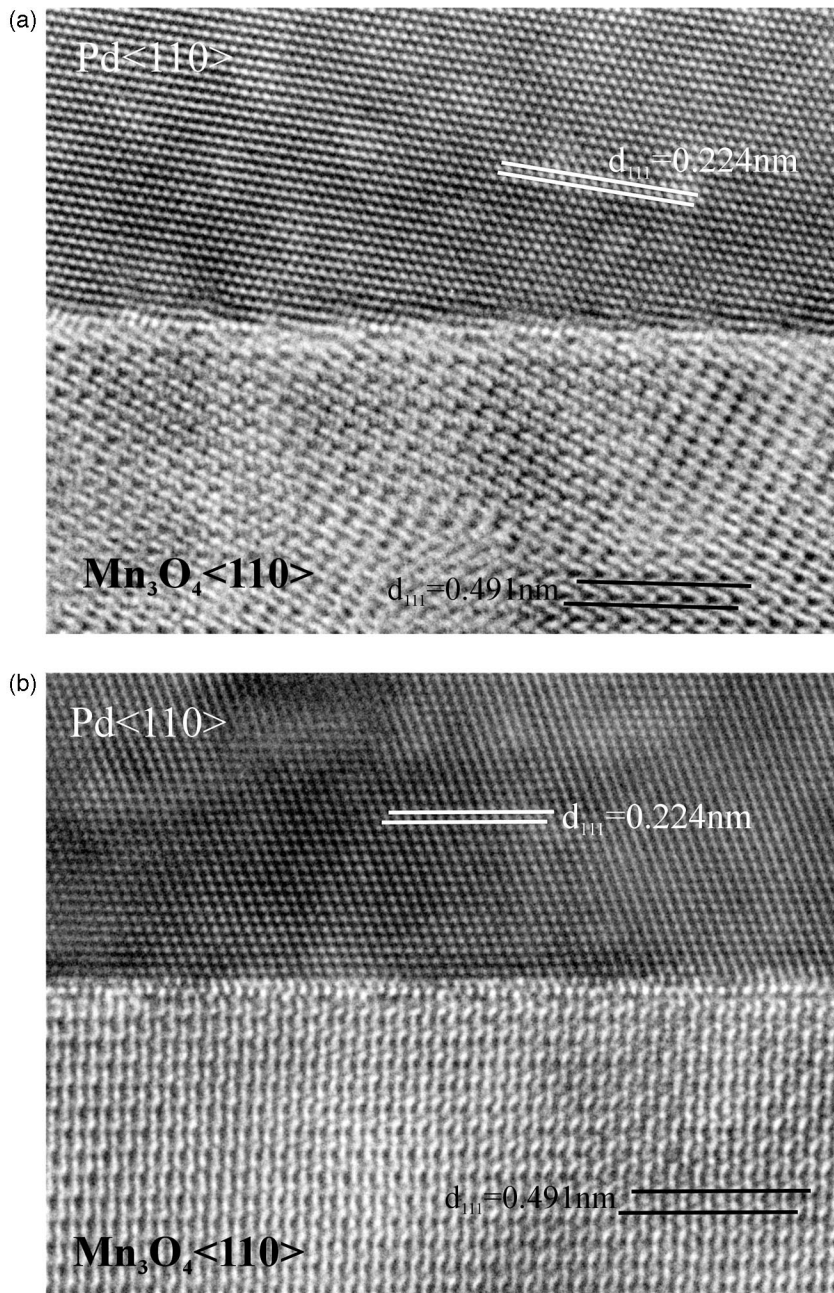
Fig. 2. HRTEM images of the edge-on observed {111} interfaces of the Mn$_3$O$_4$ precipitate in Pd as shown in Fig. 1. In (a) the tilt of 7.6° between {111} planes of Mn$_3$O$_4$ and Pd is clearly illustrated; the tilt is relieved by ledges in the Pd with height 1/4⟨112⟩ and direction ⟨110⟩ (i.e. parallel to the ⟨110⟩ viewing direction). In (b) the interface with parallel {111} planes of Mn$_3$O$_4$ and Pd is shown.

the six ⟨110⟩ that are perpendicular to the c-axis). In contrast, for the parallel +7.6°-tilted {111} interfaces, only 1/6 of Pd⟨110⟩ and Mn$_3$O$_4$⟨110⟩ are still parallel. All of these observations for Mn$_3$O$_4$ octahedrons in Pd are exactly similar to the observations for Mn$_3$O$_4$ octahedrons in Ag [28–31]. However, two important differences occur: (1) the Mn$_3$O$_4$ are larger by a factor of about 10 in Pd than in Ag; and (2) the (002) truncation of the octahedrons is substantial in Pd (see Fig. 1) and not in Ag. In fact, truncation in Ag only

becomes present after annealing *in vacuo* [33]. The larger size of Mn$_3$O$_4$ precipitates in Pd than in Ag is caused by the much lower oxygen permeability ($c_O D_O$, with c_O being the solubility and D_O the diffusion coefficient of oxygen in the metal matrix) in Pd than in Ag [34]. Oxygen permeates through Pd more slowly so that the Mn has more time to develop into larger oxide precipitates. Generally, a smaller difference in oxygen affinity between the metallic element to be oxidized and the metal of the matrix is
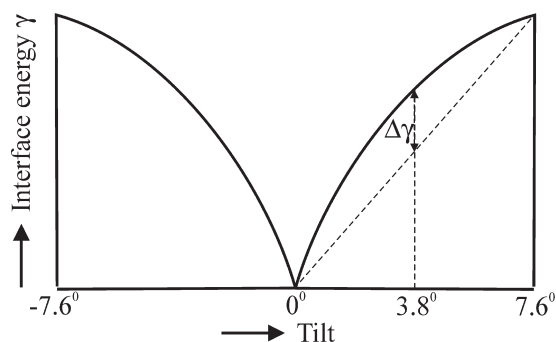
Fig. 3. Interface energy γ as a function of tilt angle between {111} planes of Mn_3O_4 and Pd. The introduction of ledges in Pd to relieve the tilt will result in a concave-shaped dependence of interface energy on tilt angle. Due to this dependence, a precipitate with one pair of facets with {111} of Mn_3O_4 and Pd aligned parallel and the other pair showing a tilt of 7.6° is in a lower-energy state than a precipitate with all four interfaces showing a tilt of 3.8°.

responsible for larger precipitates, but this argument does not hold for the present difference in sizes of the Mn_3O_4 precipitates in Pd and Ag.

Besides the octahedron-shaped precipitates, which comprise about 2/3 of all of the precipitates, plate-like precipitates were observed, comprising the rest. When viewing along the Pd⟨110⟩ direction, plates were observed along the Mn_3O_4⟨110⟩ direction with edge-on interfaces as shown in Fig. 4 together with the corresponding SAED pattern. According to the combined information of the SAED pattern and bright-field image, and according to HRTEM images (see Fig. 5), the c-axis lies in the plane of projection, parallel to the cube axis of Pd and perpendicular to the dominant facet of the plate. This turned out to be the case for all edge-on observed plates when viewing along Pd⟨110⟩. Also, inclined plates making a projected angle of about 90° with the edge-on plates were observed when viewing along the Pd⟨110⟩ direction (see Fig. 6). In this case an a-axis of Mn_3O_4 is in the plane of projection parallel to a cube axis of Pd. The Mn_3O_4⟨011⟩ zone axis appeared to be rotated by about 4° with respect to Pd⟨110⟩ around the common a-axis/cube axis in the plane of projection. The orientation of both the edge-on and the inclined plates is rather expected. Viewing along Pd⟨110⟩, one cube axis of Pd is in the plane of projection and the two other cube axes are inclined 45° with respect to the plane of projection. The c-axis of Mn_3O_4, always the normal of the plates, can be parallel to either one of these three Pd cube axes. So, 1/3 of the plates will be observed edge-on and 2/3 of the plates will be inclined 45° with respect to the projection plane when viewing along Pd⟨110⟩. Parallelism of principal axes of Mn_3O_4 and cube axes of Pd implies that ⟨110⟩Mn_3O_4 lies parallel to ⟨110⟩Pd (for the 1/3 edge-on plates), whereas ⟨011⟩Mn_3O_4 is rotated by 4.16° with respect to ⟨011⟩Pd as observed for 2/3 of the inclined plates. The rotation of 4.16° has the same probability of being negative or positive. However,

observations of these rotations for inclined plates in a certain region indicated that the majority of plates showed a rotation in only one direction. Similarly, when observing Pd along ⟨100⟩, 1/3 of the plates are expected to lie in the plane of projection and 2/3 of the plates are edge-on. In the latter, one half should make an angle of 90° with the other half. However, again in several regions it was observed that the plates are not evenly distributed over the three possibilities, but choose collectively for one of the three options. An example is shown in Fig. 7, where an overview is given for a Pd grain projected along its cube axis. Apparently, there exists some sort of collective process when the plates nucleate, e.g. driven by growth conditions or long-range stresses, such that parallel alignment of plates is more favourable than an even distribution of the plates over the three possible (in principle) equal orientations making mutual angles of 90°.

The mismatch between inter-planar distances in Mn_3O_4 and Pd is relatively large. The a-axes of Mn_3O_4 are 4.6% longer than twice the lattice constant of Pd and the c-axis is 21.1% longer than twice the lattice constant of Pd. Comparing the fct O sublattice of Mn_3O_4 and the fcc Pd lattice, this factor of 2 drops. The c-axis of Mn_3O_4 makes the largest mismatch with directions in Pd and, from the point of view of minimizing strain/mismatch on interfaces, it is clear that the Mn_3O_4 facet with its normal as the c-axis is preferred. This possibly explains the occurrence of the plate-shaped precipitates with the Mn_3O_4 c-axis as habit plane normal. A detailed analysis of the balance between interfacial and strain energy is given in the Discussion.

The manner in which the mismatch is coped with (i.e. the state of coherency) at the (002)Mn_3O_4∥(002)Pd interfaces is of particular interest. In this respect, the detailed analysis based on HRTEM images of the state of coherency at the relatively similar Ag{002}∥MgO{002} interface as obtained by molecular beam epitaxy (MBE) [35] serves as a model. There, the mismatch is 3.1% whereas in the present case it is 4.6% (isotropic over the interface). According to predictions of the O lattice [36], for this type of interface a square network of edge dislocations is expected with line direction ⟨110⟩ and Burgers vector 1/2⟨110⟩. Analysis of the plane bending observed in HRTEM images for viewing along Ag⟨100⟩∥MgO⟨100⟩ indicated, according to [35], that instead edge dislocations with line direction ⟨100⟩ and Burgers vector 1/2⟨100⟩ were present. In the ⟨110⟩ network the O points correspond to Ag atoms atop of O atoms, but in the ⟨100⟩ network the O points correspond to Ag atoms atop of both O and Mg atoms. The latter network can be conceived as a dissociation of the former network, where the dissociation starts at the dislocation nodes positioned atop the Mg atoms and results in square stacking-faulted regions. A square dislocation network results where the correctly stacked (Ag atop of O) and stack-
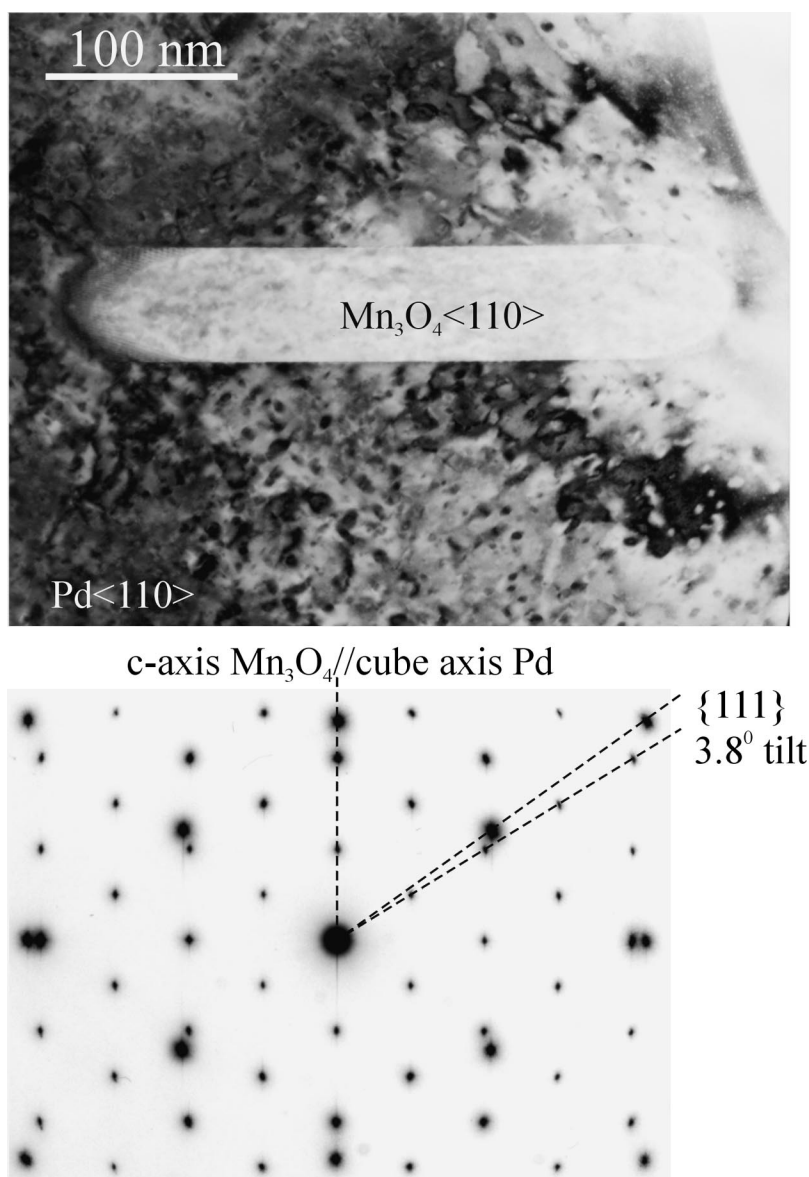
Fig. 4. Bright-field TEM image (top) and corresponding SAED pattern (bottom) of a plate-shaped Mn_3O_4 precipitate in Pd as viewed along their common $\langle 110 \rangle$ axis. For the dominant interface of the plate, (002) of Mn_3O_4 is parallel to a cube plane of Pd.

ing-faulted (Ag atop of Mg) regions alternate forming a checkerboard pattern. This alternation of correctly stacked and stacking-faulted regions was also observed for parallel {111} interfaces formed by NaCl-type oxide precipitates and an fcc metal matrix [30, 37], as well as for the parallel {111} Ag/Mn_3O_4 interface [28–31]. However, for these latter interfaces, stacking faults do not imply incorrect bonding across the interface with first-nearest neighbours as for the parallel {200}, but only an incorrect *orientation* of the bonds for atoms two {111} planes apart across the interface. Hence, the stacking-fault energy in the latter case is expected to be low [37].

To enable a detailed analysis of the possible type of dislocation network at the parallel (002) Pd/Mn_3O_4 interface, HRTEM images of the edge-on oriented interfaces were recorded along both the $\langle 110 \rangle$ and $\langle 100 \rangle$ viewing directions of $Pd\|Mn_3O_4$. Examples are shown in Fig. 8(a) and (b), respectively, where the images are contracted by a factor of 3 more or less perpendicular to the interface to mimic a grazing angular view of the planes continuing across the interface. In this way, the coherency across the interface can be observed more easily. For the images taken along $\langle 110 \rangle$ it is clear that coherency across the interface is maintained for the main part of the projected interface length, whereas the regions where the misfit dislocations are concentrated are of relatively shorter lengths. These latter regions are encircled in Fig. 8(a). On the other hand, for the images taken along $\langle 100 \rangle$,
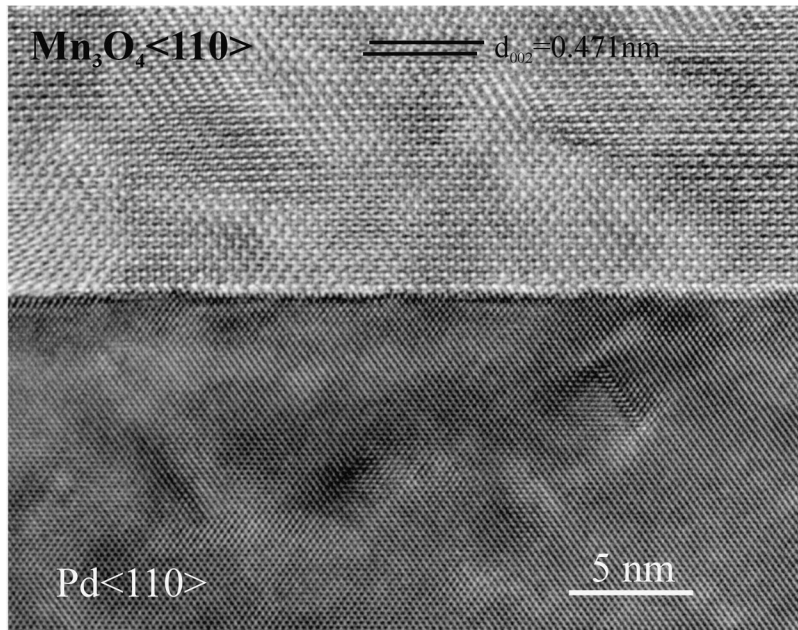
Fig. 5. HRTEM image showing the dominant interface of a plate-shaped Mn_3O_4 precipitate, with (002) of Mn_3O_4 parallel to a cube plane of Pd.
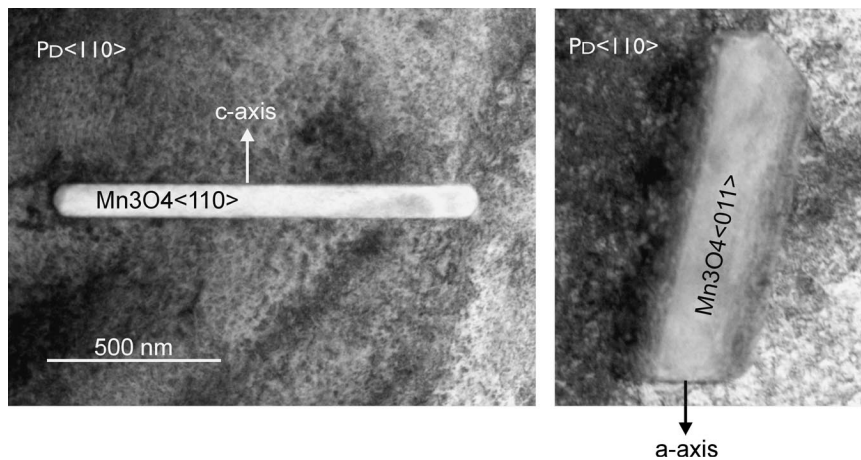

Fig. 6. Bright-field TEM image of the two orientations of Mn_3O_4 plates in Pd when viewed along the Pd$\langle 110 \rangle$ axis. Since in this case one of the cube axes of Pd is in the plane of projection and the other two cube axes are inclined 45° with respect to the viewing direction, and since the c-axis of Mn_3O_4 (which is the normal of the plate) is parallel to either one of these three cube axes, 1/3 of the precipitates will be observed edge-on (left image) and 2/3 of the plates will be inclined 45° with respect to the viewing direction (right image). Both images stem from the same Pd grain and are shown with their correct mutual orientation.

the portion in which the disregistry along the interface is concentrated is rather large compared with the other regions where the planes across the interface match smoothly. Again, the regions where the disregistry is concentrated are encircled in Fig. 8(b). The relative projected lengths of these regions are a consequence that either one array of the dislocation lines is observed edge-on with the other array running perpendicular to the viewing direction (giving a short length), or (the other possibility) that both arrays are inclined by 45° with respect to the viewing direction (giving a larger length). Discrimination between the

square networks of either $1/2\langle 110 \rangle$ or $1/2\langle 100 \rangle$ type of Burgers vectors can be made by realizing that the former gives a disregistry along small regions for observation along $\langle 110 \rangle$ and along larger regions for observation along $\langle 100 \rangle$. In the latter network the relative sizes of these regions are reversed. Hence, from our experimental observations it is clear that networks with line direction $\langle 110 \rangle$ and Burgers vector $1/2\langle 110 \rangle$ are present at the interfaces. Comparing the atomic positions in MgO{200} and Mn_3O_4(002) as shown in Fig. 9(a) and (b), respectively, indicates that the analogously stacking-faulted regions with Ag atop of Mg
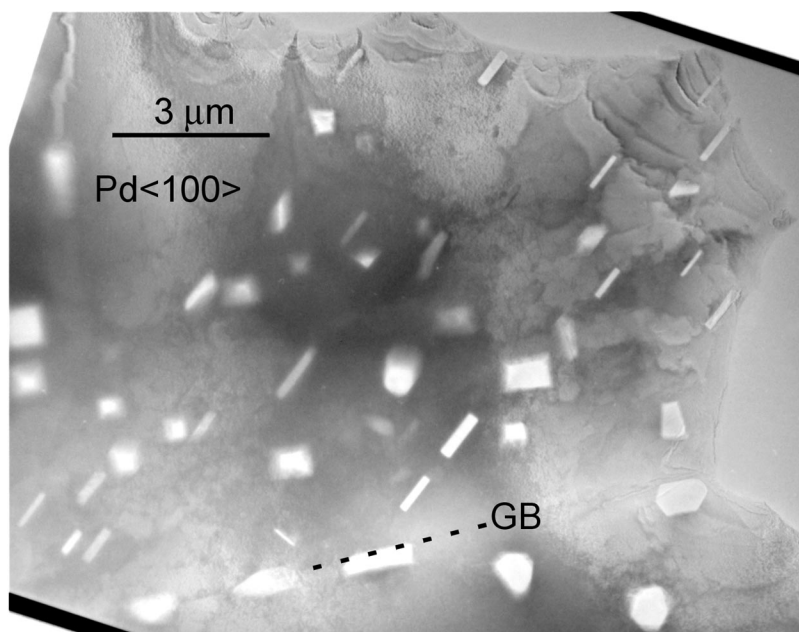
Fig. 7. Bright-field TEM image showing a large overview of Mn_3O_4 precipitates in Pd for viewing along Pd$\langle 100 \rangle$. On average, 1/3 of the plate precipitates should be parallel to the plane of projection and 2/3 should be seen edge-on. Of this 2/3, half of the plates should make an angle of 90° with respect to the other half. The image shows that the plate precipitates do not distribute equally over these three identical possibilities. Apparently, the conditions of growth and (for example) long-range stresses induce a collective process in which the plates tend to be oriented parallel.
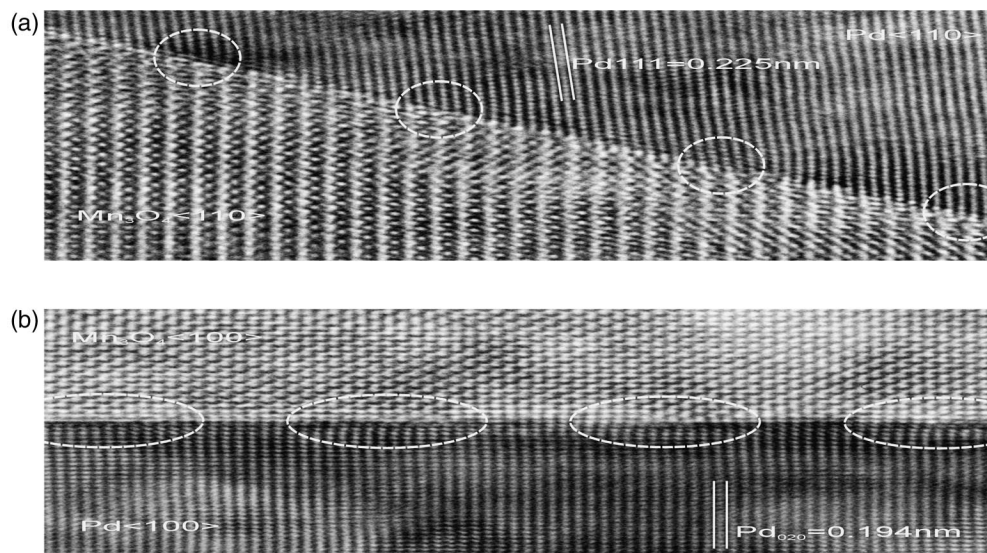
Fig. 8. HRTEM images contracted more or less perpendicular to the interface of a plate-shaped precipitate with (002) of Mn_3O_4 parallel to {200} of Pd for viewing along $\langle 110 \rangle$ (top image) and $\langle 100 \rangle$ (bottom image). Regions at the interface of disregistry, i.e. where the planes of Mn_3O_4 and Pd across the interface do not continue in a matched fashion, are encircled. Relatively small regions of disregistry are observed for viewing along $\langle 110 \rangle$ and large regions for viewing along $\langle 100 \rangle$. These observations indicate the presence of a rectangular network of edge-type misfit dislocations with line direction $\langle 110 \rangle$ and Burgers vector of $1/2\langle 110 \rangle$.

do not make sense for the Pd atop of Mn, because only half of these positions occur and the other half corresponds to Pd atop of interlocking positions in between squares of O atoms. To keep Pd atop of the O atoms, the $1/2\langle 110 \rangle$ type network suffices and dissociation of this network is not beneficial.

4. DISCUSSION

NaCl structure-type oxides (e.g. MgO, MnO, CdO, NiO) as grown by internal oxidation in fcc metals are predominantly present in octahedrally shaped precipitates bounded by parallel {111} planes of both metal

MgO(002) 2x2 unit cells

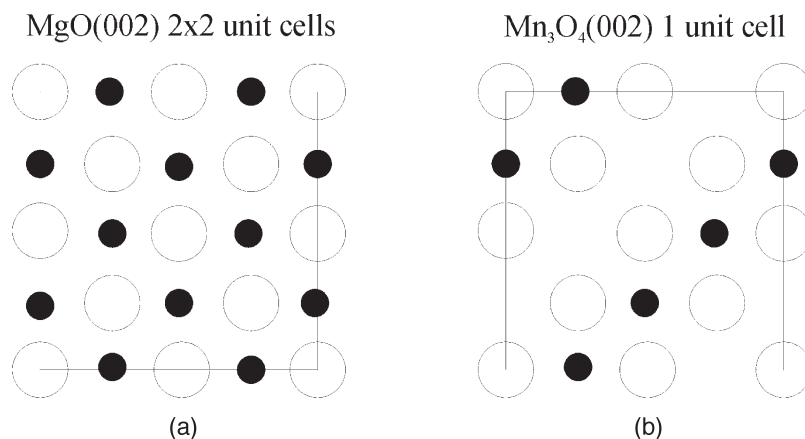## Mn₃O₄(002) 1 unit cell

(a)

(b)

Fig. 9. (a) {200} plane of NaCl-type oxides such as MgO and MnO and (b) the corresponding (002) plane in Mn₃O₄.

and oxide [19–22,24–30]. In the oxide {111} corresponds to a polar interface. These observations seem to be rather independent of the precise character of the surrounding metal; that is to say, not affected by the misfit between metal and oxide and by the detailed electronic band structure. The relative stability of these interfaces is related to the bonding established across the interface. Strong evidence comes from *ab initio* calculations on adhesive energy and charge transfer for MgO/Cu hetero-interfaces (corresponding to parallel topotaxy between MgO and Cu), where two types of {111} polar interface (O- and Mg-terminated oxide) and two types of {100} non-polar interface (with either O or Mg directly atop of Cu) were considered [38]. The Cu in-plane lattice constant was stretched to match that of MgO, giving a coherent interface (and these calculations do not allow any insight into the role of strain). The polar interfaces were shown to exhibit significantly larger adhesive energies and charge transfer than the non-polar interfaces. Further, the O-terminated {111} interface was more stable than the Mg-terminated one. The mismatch between these fcc metals and NaCl structured oxides is usually quite large and closely spaced misfit dislocations are generated [19–21,24–30]. Consequently, the influence of misfit on the energy of facets cannot be deduced because it will be largely similar for all possible types of facet and hence does not result in observable deviations from the shape according to the Wulff energy construction in the absence of misfit.

In this respect Mn₃O₄ precipitates in fcc metal matrices become interesting, because a strong anisotropy component in misfit is added. The oxygen sublattice of Mn₃O₄ is fct with c-axis 15.7% longer than its a-axis. Therefore it corresponds to a tetragonal distortion of the fcc O sublattice of the NaCl-type oxides. The a-axis of the fct O sublattice of Mn₃O₄ is near to or slightly larger than the lattice constant of most of the fcc metals, whereas the c-axis is substantially larger. Hence, the expected shape of

the Mn₃O₄ precipitates in these fcc metals complying to minimum misfit on the interfaces is plates, with the c-axis as habit plane normal. So, an interesting competition between the interfacial binding energy that favours the {111} type interfaces and the misfit energy that favours the (002) facets will occur for Mn₃O₄ precipitates in fcc metals. Note that misfit energy in the present sense does not refer to the strain energy of coherent inclusions that acts throughout the volume of a particle and part of the surrounding matrix, but to the network of misfit dislocations that have largely cancelled the long-range stresses. Misfit between precipitate and matrix now does not act on the volume of the precipitate, but on a localized region near the interfaces. In this case, the influence of the mismatch in principle is an integral part of the interfacial energy. However, in order to make our point clear in the present discussion, we have to make a distinction with the interfacial energy that is present in the absence of strain according to the Wulff construction. To keep the two contributions to the interfacial energy clear in the rest of the paper, the former is called misfit energy and the latter interfacial binding energy.

The plate-shaped Mn₃O₄ precipitates complying to a minimum misfit energy (i.e. a minimum misfit dislocation density) were *not* observed in either Ag or Cu [28–31]. In fact, only the octahedrally shaped precipitates were observed, just like the ones of NaCl-type oxides in fcc metal matrices. Apparently, in establishing the shape of the precipitate in these systems, the anisotropy in interfacial binding energy seems to be more important than the anisotropy in misfit energy. Arguments for the strong preference for parallel {111} type interfaces compared with parallel (002) interfaces have been given previously [28–31]. In fact, combining misfit and interfacial binding energy, (002)-truncated octahedrons are expected. In Ag after internal oxidation only a small fraction (i.e. less than 1%) of the precipitates showed large (002) facets, whereas the rest showed no observable trunc-

ation [28–31]. However, after annealing for 1 week in vacuum (at 650°C), almost all octahedrons showed small (002)-truncated octahedrons [33]. So, for Mn_3O_4 in Ag, there is some evidence that growth promotes the presence of {111} and reduces the possibility of (002) interfaces to form. Actually, in contrast to Ag, Cu is not suitable for the present discussion since the Mn_3O_4 in this matrix is formed from MnO [31]. The original shape of the MnO precipitate in Cu largely determines the final shape of the Mn_3O_4 precipitates without leaving room for any significant influence of the misfit between Cu and Mn_3O_4 on the shape.

Analogously to the situation in Ag, Mn_3O_4 in Pd nucleates directly and so these systems are comparable. Interestingly, besides the similarity that octahedrons form preferentially with {111} of metal and oxide parallel for one pair of facets and 7.6°-tilted for another pair of facets, also a clear difference between Pd and Ag occurs. In contrast to Ag, plate-like precipitates with the Mn_3O_4(002) habit plane could be found in Pd. Although the predominant type of precipitate is still octahedrally shaped, a significant fraction, i.e. about 1/3 of the precipitates, shows this plate-like shape. Further, the octahedrally shaped precipitates show a relatively large (002) truncation in Pd compared with Ag, indicating for Pd the increased stability of this type of interface compared with the {111} type.

Several factors, different for Ag and Pd, may explain the transition from a state where misfit is not important [i.e. precipitates *without* significant (002) facets in Ag] to a state where the energy difference due to misfit becomes similar in magnitude to the interfacial binding energy difference between parallel/tilted {111} and parallel (002) interfaces [i.e. to precipitates *with* significant (002) facets in Pd].

A first obvious reason might be the mismatch between metal and oxide; that is to say, it increases going from the Ag to the Pd system because the lattice constant of Pd is 4.8% smaller than that of Ag. Hence, the energy related to misfit increases. However, this increase occurs for both the (002) and the {111} type interfaces. For the semi-coherent interfaces presently considered, the misfit dislocation density increases by the same amount for both types of interface. So, as a first-order estimate, the difference in misfit energy between these two interface types does not change with respect to the difference in interfacial binding energy. Hence, in itself, this cannot explain the increased stability of the (002) type interface for the Pd system.

Second, the size of the Mn_3O_4 precipitates is 10 times larger in Pd than in Ag. For increasing size of coherent precipitates the elastic strain energy (scaling with volume) becomes increasingly more important compared with interfacial energy, which scales with the interface area [7, 8], and thus the increase in interfacial energy upon loss of coherency is outweighed by the decrease in elastic strain energy. In

this respect it is noteworthy that for the present oxide precipitates, i.e. with a large mismatch with the metal, semi-coherent interfaces are formed right from the outset. In this sense, loss of coherency will not occur. As shown in Section 3 and [28–31], the interfaces between Mn_3O_4 and both Pd and Ag are semi-coherent. Hence, the argument—that due to an increase of the size of the precipitate the influence of strain energy becomes larger—does not hold. Assuming that the networks of misfit dislocations cancel the long-range stresses, the energy associated with the misfit and with the interfacial binding energy now both scale with the interface area. Still, also for an incoherent inclusion, due to the size difference between the unstrained inclusion and the "hole" in the matrix, strains throughout the volume of the inclusion are possible [39]. However, for the oxide precipitates grown in a metal matrix at a temperature relatively near to the melting point of the metal and using vacuum annealing to allow some equilibration, these strains are not expected to be important. During cooling thermal mismatch between oxide and matrix will occur, but is not of influence on the precipitate shapes observed. However, cooling can be responsible for the tetragonal twinning observed within the Mn_3O_4 precipitates.

A third reason has to do with the difference in elastic constants of Pd and Ag. One should realize that Pd is substantially stiffer than Ag. The shear modulus of Pd (53.2 GPa) is larger by a factor of almost 1.6 than that of Ag (33.8 GPa), and approaches the stiffness of MnO (68 GPa) [40]. These elastic constants affect the values of the interface dislocation energy factor, i.e. the misfit energy, to a large extent. The elastic energy per unit length of the interface dislocation is given by (Einstein convention):

$$E = \frac{1}{4\pi i}\sum_\eta \frac{L_{r\eta}L_{s\eta}b_r b_s}{A_{m\eta}L_{n\eta}}\ln\left(\frac{R}{r_c}\right). \qquad (1)$$

The pre-logarithmic factor, i.e. the so-called energy factor K, for a heterophase interface depends, in contrast to a homophase interface (grain boundary), directly on the various elastic constants and also indirectly via the magnitude of the Burgers vector, b. $L_{n\eta}$ and $A_{m\eta}$ correspond to Lekhnitskii's representation that is valid for the general anisotropic case [41], which are basically the very same vectors as introduced by Stroh [42]. r_c is the cut-off radius of the dislocation core and R represents half the distance between the interface dislocations. Taking into account the constraints on the continuities in displacements and tractions, the distribution of the Burgers vector in the absence of external forces and the pre-logarithmic factors can be calculated explicitly for $1/2\langle 110\rangle$ interface dislocations on {100} and {111} planes [43, 44]. The results are listed in Table 1 using the elastic constants of MnO. Note that, in this section, MnO with isotropic mismatch is used and not

Table 1. Pre-logarithmic energy factors K (eV/nm) and fractions of the Burgers vector for $1/2\langle110\rangle$ dislocations at $\{100\}$ and $\{111\}$ interfaces between Pd/MnO and Ag/MnO

	K (eV/nm)		Fraction b in metal	Fraction b in oxide
	$\{100\}$	$\{111\}$		
Pd	3.48	3.32	0.55	0.45
Ag	2.92	2.72	0.66	0.34

Mn_3O_4 with anisotropic mismatch due to its tetragonal axes. As expected, the components of the Burgers vectors are almost equally distributed over the metal and the oxide in the case of Pd/MnO. As a matter of course one should bear in mind that the Burgers vector is actually a translational vector for only one of the half-crystals and it cannot move in the other crystal, neither by climb or glide, without creating high-energy stacking faults. A larger difference in Burgers vector distribution appears for the Ag/MnO system because Ag is the more compliant material. The pre-logarithmic factors for $1/2\langle110\rangle$ interface dislocations on $\{100\}$ and $\{111\}$ planes in the Pd/MnO system are also larger than those in the Ag/MnO system. These values are employed to calculate the interface energy (i.e. only the misfit energy part) due to non-interacting interface dislocations as a function of the isotropic misfit for Pd/MnO and Ag/MnO, as displayed in Fig. 10(a) and (b), respectively. The interface energy for $1/2\langle110\rangle$ interface dislocations in Pd/MnO is always larger than in Ag/MnO, for either $\{100\}$ or $\{111\}$ interface planes. Although in this section MnO is used instead of Mn_3O_4, the calculations are certainly useful to draw the following conclusion about interfaces between Mn_3O_4 and either Pd or Ag. Because of the higher pre-logarithmic factors of Pd, the extra dislocations needed to relieve the larger misfit at the $\{111\}$ compared with the (002) type interface will cost more energy in the Pd than in the Ag system. Hence, in the Pd system, the (002) type interfaces become relatively more stable, explaining the increased (002) truncation of the octahedrons and the presence of the plate-shaped precipitates.

Although in this discussion we treated the misfit and the interfacial binding energy separately, the bonding across the interface is essential to generate the dislocation networks associated with the misfit energy. Based on a comparative study [45, 46] between an anisotropic elasticity and an atomistic approach, we concluded that the elasticity curve of Fig. 10 connects points with different interaction parameters (specifying the bonding strength across the interface); that is to say, with a higher value at higher misfit. This means that at higher values of mismatch it takes a larger interaction to arrive at dislocation-like structures. Indeed, the Pd–O bond strength is higher than the Ag–O bond strength and, as a
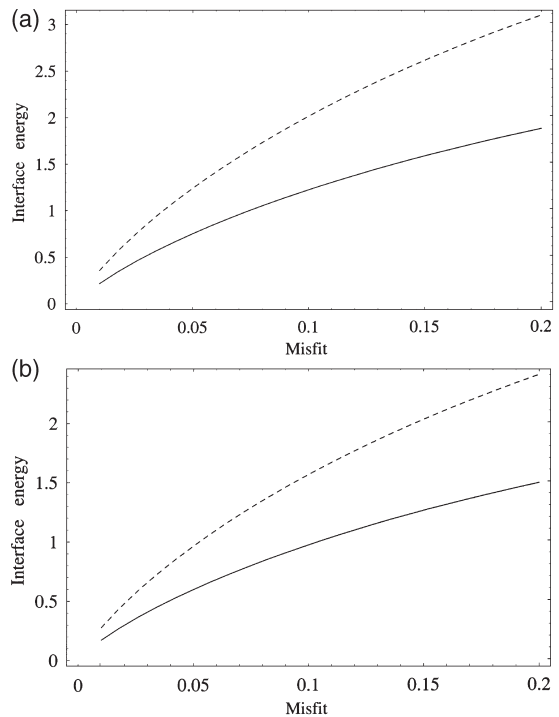

Fig. 10. (a) Interface energy of $1/2\langle110\rangle$ non-interacting interface dislocations on $\{100\}$ (solid) and $\{111\}$ (dashed) planes in the Pd/MnO system as a function of lattice mismatch. (b) Energy of $1/2\langle110\rangle$ non-interacting interface dislocations on $\{100\}$ (solid) and $\{111\}$ (dashed) planes in the system Ag/MnO as a function of lattice mismatch.

consequence, the coupling strength across the Pd/Mn_3O_4 interface is high enough to generate interface dislocations on both the $\{111\}$ and (002) interfaces. The electronic bonding due to 2sp O/4d Pd hybridization of Pd–O is not available for Ag–O and a weaker bond will be formed. In the latter the binding may be attributed to the Coulomb interaction between the ions in the oxide and the "image charges" in the metal, or rather the charge density that they induce in the metal. Here only distributions with a wavelength equal to or larger than the Fermi wavelength are permitted. Because of the possibility of screening of the localized ionic charges by the outer 5s electrons of Ag, no strong "chemical" bonds will be formed across the interface as in the case of Pd/Mn_3O_4. The consequence is that the (unreconstructed) polar $\{111\}$ surface of the oxide, which has a dipole in the repeat unit perpendicular to the interface giving rise to a diverging surface energy [47], is stabilized more strongly by Pd and less by Ag.

Although its contribution is of secondary importance, it should be realized that also the intrinsic stacking-fault energy of Pd is larger than that of Ag, 180 versus 17 mJ/m^2 [48]. For the $\{111\}$ type interface, regions with correct fcc stacking and with local hcp stacking (i.e. a stacking fault at the interface) alternate [27–31,37]. For the (002) interface with a square net of $1/2\langle110\rangle$ edge-type misfit dislocations,

stacking faults at the interface do not occur. Thus, an increased stacking-fault energy of the metal neighbouring the oxide may thus also decrease the stability of the {111} with respect to the (002) type interface.

So, the general conclusions of the present analysis are: (1) the anisotropy in interfacial binding energy for oxide precipitates in a metal matrix is substantial due to the ionic nature of the oxide, giving well-defined shapes associated with the Wulff construction, i.e. parallel {111} interfaces for NaCl-type oxides in an fcc metal matrix; and (2) the influence of misfit on the precipitate shape as bounded by semi-coherent interfaces is important only if sufficient anisotropy in mismatch is present and if the matrix is sufficiently stiff. For a soft matrix (exemplified by Ag) the influence of mismatch is hardly present, despite a strong anisotropy in mismatch, whereas for a relatively stiff metal like Pd the strain energy becomes similar in magnitude to the interfacial energy.

5. CONCLUSIONS

Internal oxidation of Pd–3 at.% Mn in air at 1000°C results in Mn_3O_4 precipitates present with two types of dominant shape. One type is octahedrally shaped and bounded by {111} of the Mn_3O_4. These close-packed oxygen planes want to be parallel to close-packed palladium planes, but actually—due to the tetragonality of Mn_3O_4—only for one pair of facets can this parallelism be achieved. At the other facets the tilt between the {111} planes of metal and oxide is relieved by ledges in the Pd with direction $\langle 110 \rangle$ and height $1/4\langle 112 \rangle$. These observations are identical for Mn_3O_4 precipitates in Ag; however, the octahedrons show relatively larger truncation by (002) in Pd than in Ag. Further, the second type of precipitate shape, comprising about 1/3 of all of the precipitates in Pd, was not observed in Ag. It corresponds to a plate-like structure, showing an orientation relationship where the tetragonal axes of Mn_3O_4 are parallel to the cube axes of Pd, with the c-axis of Mn_3O_4 as habit plane normal. HRTEM observations revealed the presence of a square misfit dislocation network with line direction $\langle 110 \rangle$ and Burgers vector $1/2\langle 110 \rangle$ at these interfaces with $(002)Mn_3O_4\|\{200\}Pd$. Since the c-axis of Mn_3O_4 gives the largest mismatch with Pd (21.1% compared with 4.6% along the a-axes), the observed plate-like shape corresponds to a minimum misfit energy. However, the precipitate shape corresponding to a minimum interfacial binding energy is an octahedron bounded by {111}. So, the final shape is determined by the competition between misfit and interfacial binding energies. Due to the increased stiffness of the Pd compared with the Ag matrix, the difference in misfit energy becomes similar in magnitude to the difference in interfacial binding energy between parallel/tilted {111} and parallel (002) interfaces of metal and Mn_3O_4. This explains the larger (002)

truncation of the octahedrons in Pd, and the presence of the plate-like Mn_3O_4 precipitates in Pd and their absence in Ag. It can be concluded that the stronger coupling strength due to Pd–O bonds across the interface leads to formation of the dislocation network structures at larger misfit compared with the situation with Ag.

REFERENCES

1. Sutton, A. P. and Balluffi, R. W., *Interfaces in Crystalline Materials*. Oxford University Press New York, 1996.
2. Wulff, G., *Z. Kristallogr.*, 1901, **34**, 449.
3. Johnson, C. A. and Chakerian, G. D., *J. Math. Phys.*, 1965, **6**, 1403.
4. Kato, M. and Fuji, T., *Acta metall. mater.*, 1994, **42**, 2929.
5. Kato, M., Fuji, T. and Onaka, S., *Acta metall. mater.*, 1996, **44**, 1263.
6. Eshelby, J. D., *Proc. Roy. Soc. A*, 1957, **241**, 376.
7. Johnson, W. C. and Cahn, J. W., *Acta metall.*, 1984, **32**, 1925.
8. Thompson, M. E., Su, C. S. and Voorhees, P. W., *Acta metall. mater.*, 1994, **42**, 2107.
9. Lee, J. K., *Metall. Mater. Trans. A*, 1996, **27**, 1449.
10. Bowles, J. S. and Mackenzie, J. K., *Acta metall.*, 1954, **2**, 124, 129, 138.
11. Nishiyama, Z. Martensitic Transformation, 1978, Academic Press, New York.
12. Dahmen, U., *Acta metall.*, 1982, **30**, 63.
13. Dahmen, U. and Westmacott, K. H., *Acta metall.*, 1986, **34**, 475.
14. Duly, D., *Acta metall. mater.*, 1993, **41**, 1559.
15. Dahmen, U., Ferguson, P. and Westmacott, K. H., *Acta metall.*, 1984, **32**, 803.
16. Luo, C. P., Dahmen, U. and Westmacott, K. H., *Acta metall. mater.*, 1994, **42**, 1923.
17. Finnis, M. W., *Acta metall. mater.*, 1992, **40**, S25.
18. Duffy, D. M., Harding, J. H. and Stoneham, A. M., *Phil. Mag. A*, 1993, **67**, 865.
19. Merkle, K. L., *Ultramicroscopy*, 1991, **37**, 130.
20. Mader, W., *Z. Metallkd.*, 1992, **83**, 7.
21. Ernst, F., *Mater. Sci. Eng. Rep.*, 1995, **R14**, 97.
22. Ernst, F., Pirouz, P. and Heuer, A. H., *Phil. Mag.*, 1991, **63**, 259.
23. Lu, P. and Cosandey, F., *Ultramicroscopy*, 1992, **40**, 271.
24. Jang, H., Seidman, D. N. and Merkle, K. L., *Interface Sci.*, 1993, **1**, 61.
25. Chen, F. R., Chiou, S. K., Chang, L. and Hong, C. S., *Ultramicroscopy*, 1994, **54**, 179.
26. Vellinga, W. P. and De Hosson, J. Th. M., *Mater. Sci. Forum*, 1996, **207-209**, 361.
27. Chan, D. K., Seidman, D. N. and Merkle, K. L., *Phys. Rev. Lett.*, 1995, **75**, 1118.
28. Kooi, B. J., Groen, H. B. and De Hosson, J. Th. M., *Acta mater.*, 1997, **45**, 3587.
29. Kooi, B. J., Groen, H. B. and De Hosson, J. Th. M., *Acta mater.*, 1998, **46**, 111.
30. De Hosson, J. Th. M., Groen, H. B., Kooi, B. J. and Vitek, V., *Acta mater.*, 1999, **47**, 4077.
31. Kooi, B. J. and De Hosson, J. Th. M., *Acta mater.*, 1998, **46**, 1909.
32. Wyckoff, R. W. G., *Crystal Structures*. Interscience Publishers New York, 1963.
33. Kooi, B. J., Westers, A. R., Vreeling, J. A., van Agterveld, D. T. L. and De Hosson, J. Th. M., *Mater. Sci. Forum*, 1999, **294-296**, 255.

34. Meijering, J. L., *Adv. Mater. Res.*, 1971, **5**, 1.
35. Trampert, A., Ernst, F., Flynn, C. P., Fischmeister, H. F. and Ruhle, M., *Acta metall. mater.*, 1992, **40**, S227.
36. Bollmann, W., *Crystal Defects and Crystalline Interfaces*. Springer New York, 1970.
37. Groen, H. B., Kooi, B. J., Vellinga, W. P. and M De Hosson, J. Th., *Phil. Mag. A*, 1999, **79**, 2083.
38. Benedek, R., Minkoff, M. and Yang, L. H., *Phys. Rev. B*, 1996, **54**, 7697.
39. Porter, D. A. and Easterling, K. E., *Phase Transformations in Metals and Alloys*. Van Nostrand Reinhold Company New York, 1981.
40. Simmons, G. and Wang, H., *Single Crystal Elastic Constants and Calculated Aggregate Properties: A Handbook*. MIT Press Cambridge, MA, 1971.
41. Lekhnitskii, S. K., *Theory of Elasticity of an Anisotropic Body*. Holden Day San Francisco, CA, 1977.
42. Stroh, A. N., *J. Math. Phys.*, 1962, **41**, 77.
43. De Hosson, J. Th. M., Vellinga, W. P., Zhou, X. B. and Vitek, V., *Stability of Materials. Structure–Property Relationship of Metal–Ceramic Interfaces*. Gordon Breach New York, 1996.
44. Barnett, D. and Lothe, J., *J. Phys. F*, 1974, **4**, 1618.
45. De Hosson, J. Th. M., Groen, H. B., Kooi, B. J. and Vellinga, W. P., *Advances in Electronmicroscopy*. Kluwer Dordrecht, 1999.
46. Vellinga, W. P., De Hosson, J. Th. M. and Vitek, V., *Acta mater.*, 1997, **45**, 1525.
47. Tasker, P. W., *J. Phys. C*, 1979, **12**, 4977.
48. Hirth, J. P. and Lothe, J., *Theory of Dislocations*. John Wiley and Sons New York, 1982.